PAPER

Separating strain sensor based on dual-resonant circular patch antenna with chipless RFID tag

IOP Publishing Smart Materials and Structures
Smart Mater. Struct. **30** (2021) 015007 (12pp) https://doi.org/10.1088/1361-665X/abc92d

Separating strain sensor based on dual-resonant circular patch antenna with chipless RFID tag

Guochun Wan[1], Wenhao Kang[1], Chao Wang[1], Wenzhao Li[1], Mengmeng Li[1], Liyu Xie[2] and Lan Chen[3]

[1] Department of Electronic Science and Technology, Tongji University, Shanghai, People's Republic of China
[2] Department of Disaster Mitigation for Structures, Tongji University, Shanghai, People's Republic of China
[3] School of Electrical and Electronic Engineering, Shanghai Institute of Technology, Shanghai, People's Republic of China

E-mail: chenlan@sit.edu.cn

Received 29 April 2020, revised 19 August 2020
Accepted for publication 10 November 2020
Published 1 December 2020

Abstract

In the field of structural health detection, since the sensor needs to be directly bonded to the measured object, it is difficult to stably transmit the RFID information and realize the passive wireless structure strain detection. To circumvent these difficulties, this paper innovatively proposes a dual-resonant circular microstrip patch antenna (CMPA) sensor with chipless RFID tag. The information of the RFID tag can be changed that allows the sensor to be deployed on a large scale. The separating sensor includes chipless RFID tag layer and dual-resonant CMPA layer, which can simultaneously reflect RFID tag information and strain information.The design of separated layers can minimize the resonant frequency shift of ID tags when stress is implemented on CMPA strain part. Current distribution analysis and equivalent circuit are used to study the strain size and direction. Experiments show that the offset of the resonant frequency of the sensor antenna has linear relationship with the lateral and longitudinal strains. The correlation coefficients are 0.9284 and 0.9235 respectively, and the sensitivity coefficient of the lateral and longitudinal strain is 528 MHz ε^{-1} and 384 MHz ε^{-1}. At the same time, the readability of the RFID tag information is maintained.

Keywords: dual-resonant, separating sensor, strain detection, CMPA, chipless RFID tag

(Some figures may appear in colour only in the online journal)

1. Introduction

With the service load and environmental effect, the performance of the structure will gradually degrade over time [1], so the technologies in structural health monitoring has been extensively developed over the last few decades in order to monitor and evaluate the state of the structure [2].

Among them, important indicators of structural health testing include stress and crack conditions. Various antenna sensors have been developed for Crack [3–5] and Strain [6–8]. Among them, Occhiuzzi, Paggi *et al* proposed and designed a strain sensor based on a folded radio frequency identification (RFID) antenna in 2011. The limitation of this method is that the structure of the antenna proposed and the parameters to be detected are complicated, therefore, other changes besides the change of the strain may cause interference in the power of antenna, which also affect the parameters such as the impedance and gain of the antenna. When an object is deformed by an external factor such as a load, the mutual force acting on both the front and the back of any interface inside the object is called 'internal force'. The degree of integration of the internal force, that is, the internal force received

on the unit area of the object is called 'stress'. As an important feature characterizing the state of building construction, changes in strain can cause changes in the internal structure of the building. A commonly used strain measurement method is a resistive strain gauge. Varying the change of resistance by changing the resistance of the resistor requires a lengthy and complicated wiring while achieving higher accuracy. Cracks are another important indicator of structural damage. Cracks may come from structural fatigue and various physical and chemical processes. When the crack size reaches a critical size, the structure fails and causes huge loss of personnel and property. Traditional crack detection methods include visual inspection and ultrasonic inspection, which requires manual periodic inspection, which is time consuming and labor intensive [9]. As the number of sensors increases, power supply lines and data transmission lines also increase, and wiring difficulty and cost increase. Traditional sensors used for structural health testing require cables to be laid near the structure. At the same time, the corresponding data acquisition system needs to be installed, which is limited by wire and distance, and has high human and material costs. At the same time, these instruments and equipment have requirements for the on-site environment, and it is difficult to deploy on a large scale and measure in real time.

Large-scale construction of infrastructure facilitates the development and utilization of passive wireless sensors for permanent installation and online real-time health detection [10]. Sensors based on ultra-high frequency radio frequency identification tag antennas are increasingly receiving attention from structural health monitoring. Compared with traditional wired test systems, wireless systems have low cost and are suitable for multi-point real-time monitoring of complex structures [11]. When the structure of a sudden force, such as the length of the fatigue crack reaches the threshold value, the real-time monitoring can be timely warning. It can be measured in places where manual measurement is inconvenient, such as dangerous and high temperature environments. As mentioned before, traditional measurement method always includes wiring connection, nowadays RFID is applied to such measurement task. Due to its wireless configuration,the measurement can be easier to design. Passive wireless RFID solutions have the advantages of low cost, simplicity and large operating temperature range, and have many advantages over chip-based RFID. For instance, Watters *et al* [12] proposed a passive sensor design that believes that wireless sensors can be implemented by combining sensors with passive solutions in other fields. Daliri *et al* [13] manufacture a chipless sensor based on a circular patch antenna. Mohammad *et al* [14, 15] developed an antenna sensor capable of monitoring fatigue crack growth with sub-millimeter resolution. At the same time, in terms of strain measurement, Cho *et al* [16] invented a wireless multiplying antenna sensor, and Merilampi *et al* [17] proposed a wireless strain sensor for measuring large strains. Adi Mahmud Jaya Marindra *et al* [18] proposed a crack sensor that can detect multiple defect parameters.

Due to the unknown nature of the site environment, there is randomness in the direction in which the structural stress state occurs. Ahbe *et al* [19] proposed a two-port feed dual-frequency patch antenna sensor for strain wireless measurement in two directions, measuring strain in both directions. Thai *et al* [20, 21] proposed a patch antenna sensor with a cantilever ring, and the two cantilever rings independently measure the strain in two orthogonal directions. Domestic and foreign scholars have limited research on the direction of stress. By improving the design of the patch antenna sensor, we can characterize the directivity using the dual resonant frequency characteristics. In this paper, the two resonant frequency points of the sensor are used. When the direction of stress development is different, the front resonant frequency point and the rear resonant frequency point exhibit different offset laws. As far as the current research situation is concerned, many scholars focus on verifying the feasibility of using RFID patch antennas as strain sensors and use the vector network analyzer (VNA) and other instruments to measure the drift of the resonant frequency, trying to explore the approximate linear relationship between resonant frequency and the magnitude of strain.

Structural deformation caused by structural stress or crack width variation can be transmitted to the antenna attached to the surface of the structure. Changing the size parameter of the antenna changes the effective electrical length of the antenna surface, causing the resonant frequency to shift. Therefore, a properly designed patch antenna can be used as a strain sensor or as a crack width sensor. The patch antenna can be used to measure strain and crack width variations, while the RFID tag acts as an encoder to store the encoded information of the tag. Former researches like [22, 23] has proposed a sensor with tags and circular microstrip patch antenna (CMPA) unit on just one patch for crack detection. But when the CMPA part is utilized to detect strain, a problem has to be considered: when the RFID tag is deformed, the encoded information will be affected or even disappear. To circumvent these difficulties, this paper proposes a separating double-layer antenna sensor. In other words, the sensor is divided into two parts, the chipless RFID tag layer and the dual-resonant CMPA layer. With the ID part and the sensor part separated, the resonant frequency of tags will little be influenced when stress is implemented on CMPA part. Since the RFID tag and sensor are designed in different frequency bands, the tag encoding information and the resonant frequency offset of the strain sensor antenna can be detected simultaneously from the radar cross section (RCS) spectrum. The magnitude of the stress is proportional to the offset of the resonant frequency of the strain sensor portion.

Combined with the above research, the authors developed a novel separating sensor based on dual resonant features. The sensor with two layers is placed at a stress or crack concentration, the structural member is deformed by the dual-resonant CMPA layer, and the tag-layer stores the encoded information. Different from former works,the two-layer structure can improve the accuracy of the measurement result. Additionally, layered structure reduces the impact between the label layer and the strain layer. This novel structure can be a creative attempt in antenna design. The entire passive chipless RFID detection system consists of sensors, RFID tags and broadband antenna for transmission and reception and associated readers, which designed and tested by using a monostatic RCS-based

test method. The second part introduces the sensing mechanism, mode analysis, equivalent circuit of separating sensors, RFID tags, the design of broadband antenna and monostatic RCS test system. At the same time, the sensor strain simulation was simulated and analyzed. The third part is the overall experimental introduction, analysis and improvement of the sensor. The fourth part is the conclusion and future research potential.

2. Design of passive wireless measurement system

A novel passive chipless RFID sensor with two layers using a separating two-layer structure is proposed. By adjusting the structure and size of the sensor with two layers, the tags and sensors are designed in different frequency bands. The tag encoding information and the resonant frequency offset of the sensor antenna can be detected simultaneously from the RCS spectrum. The paper will introduce the sensor design ideas and working principles in detail later. The sensor with two layers is designed with two components, as illustrated in figure 1. One part is the RFID tag part, which has the hole dug in the middle. The size of the hole is slightly larger than the maximum diameter of the dual-resonant CMPA layer. It is in the tag-layer of the separating sensor with two layers and is not strongly bonded to the CMPA structure. Specifically, these two layers are connected with Scotch tape on the test sample altogether. This weak connection can minimize the influence on the tags caused by the stress implemented on the CMPA part. That is, the tag structure will not change with the deformation of the CMPA structure. The other part is the sensor antenna part, the upper surface is a dual-resonant CMPA, and the lower surface is the ground plane.

In the construction and testing on site, as the building area and complexity increase, large-scale deployment of strain and crack sensors is required, and the number of sensors is largely used. And the strain sensor is directly attached to the surface of the structure, however, it is generally difficult to use twice after the measurement. The benefits of a separate structure allow that field sensors can be flexible placed and the RFID tag information based on quantity and location can be designed easily. Moreover, the label layer of the sensor is non-adhered to the lower layer, and deformation does not occur during the detection process, so it can be recycled and reused. As the amount of sensor usage increases, the cost can be reduced to some extent.

The system is a passive wireless system based on a monostatic RCS based detection method. The RCS of the target is a physical quantity used to quantitatively describe the intensity of the scattering of the target object. When the antenna of the radar base station emits a beam of electromagnetic waves, in the meanwhile the electromagnetic wave propagates in space to meet the measured object, part of the electromagnetic energy is reflected by the object back to the same radar base station model. This model is a single station RCS. Figure 2 shows the working mode of monostatic RCS and bistatic RCS.

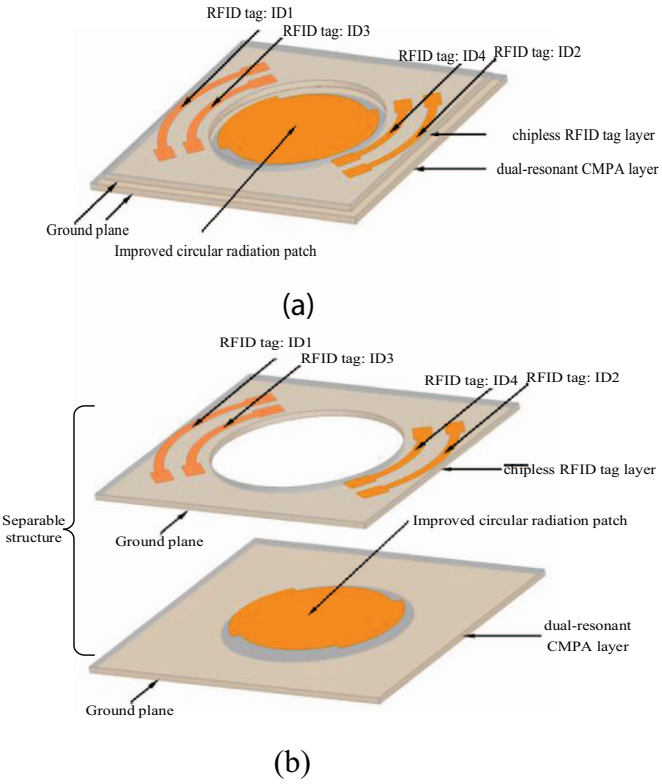

Figure 1. A novel passive chipless RFID sensor system (a) concept of separating two-layer RFID sensor system; (b) exploded view of sensor system.

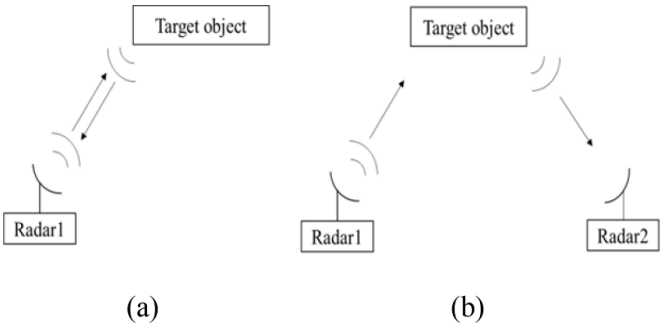

Figure 2. The working mode of monostatic RCS and bistatic RCS (a) monostatic RCS (b) bistatic RCS.

2.1. Construction of separating dual-resonant CMPA sensor with chipless RFID tag

The tag-layer of the sensor uses an improved dipole as an RFID tag. Digging holes in the center so that the information of the CMPA-layer can be detected simultaneously. In order to reduce the overall area of the separating sensor, the dipoles are redesigned in conjunction with the center digging holes. After simulation, the curved dipole structure can basically achieve the effect of the traditional dipole. Meanwhile, in order to avoid electromagnetic coupling between the dipoles, rectangular blocks are provided at both ends of the single dipole. The 4-bit RFID tag antenna in this paper works well, and the 4-bit

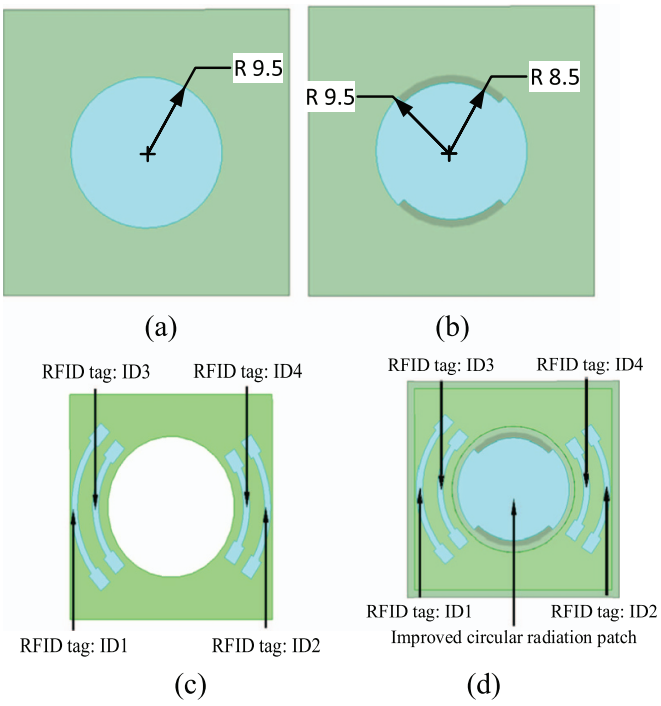

Figure 3. The front view of sensor (a) circular patch antenna; (b) improved circular patch antenna; (c) RFID tag antenna; (d) superimposed two-layer sensor.

tag information is displayed between 3 GHz and 5 GHz, which will not affect the following CMPA-layer sensor information.

The sensor based on the circular patch is shown in the figure 3(a). The operating frequency is in the basic mode, and the circular patch antenna design follows the following formula. The operating frequency is f_r in the basic mode, and the circular patch antenna design follows the following formula [24].

$$f_r = \frac{1.2412c}{2\pi R_e\sqrt{\varepsilon_r}} \tag{1}$$

$$R_e = R\sqrt{\left\{1 + \frac{2h}{\pi R\varepsilon_r}\left[\ln\left(\frac{\pi R}{2h}\right) + 1.7726\right]\right\}} \tag{2}$$

In (1) and (2), R is the radius of patch, R_e is the equivalent radius, f_r is the operating frequency; ε_r is the relative dielectric constant; h is the thickness of the dielectric substrate.

The thickness of the antenna should satisfy:

$$h \le \frac{c}{4f_m\sqrt{\varepsilon_r - 1}} \tag{3}$$

In (3), c is the speed of light, f_m is the maximum operating frequency, and ε_r is the relative dielectric constant.

As the stress sensor, although the basic structure in the figure 3(a) can detect the change in the magnitude of the stress, the directivity of the stress cannot be detected. The crack sensor is also the same. In response to this situation, the structure has been improved, and different radius fans are added on the basis of the original circular shape for pattern replenishment, as illustrated in figure 3(b). This changes the polarization characteristics and surface current distribution, so that the sensor showed dual resonant characterristics. This characteristics allows for directional characterization

The upper and lower patch antennas of the sensor use Rogers RT/duroid 5880 material as the dielectric substrate. The substrate thickness is 0.79 mm, which is one of the standard sizes. The size of the tag-layer is 33.5 mm × 33.5 mm, and the inner and outer diameters of the circular patch antenna are 17 mm and 19 mm respectively, as illustrated in figure 3(c).

The lower patch is slightly larger than the upper patch, and the CMPA-layer has a size of 36 mm × 36 mm. In order to prevent the RFID tag antenna from blocking the resonant frequency information of the lower patch strain antenna, the diameter of the middle patch hole on the upper patch is slightly larger than the maximum diameter of the disk patch of the lower patch, as illustrated in figure 3(d).

2.1.1. Modeling and simulation. After completing the antenna structure design, we need to further explore the radiation characteristics of the separating sensor with two layers. We chose to use Ansoft HFSS software for simulation, as illustrated in figure 4. It consists of an RFID tag antenna and a CMPA sensor, and an aluminum plate as a structural member. The antenna is made up of a copper sheet and a coated dielectric board. Media board material is set to Rogers RT/duroid 5880. The entire sensor with two layers is placed in a perfectly matched layer air box. At the same time, due to the monostatic RCS-based detection method, the plane wave excitation above the antenna is selected, which means the position of the RCS probe is set 10 mm above the antenna. The direction of propagation of the wave unit vector k is directed perpendicular to the antenna, and the electric field vector E0 is parallel to the patch antenna.

The monostatic RCS of the sensor with two layers in a wide range is shown in the figure 5. The RCS curve produces two sets of resonant frequencies in the frequency range. The first group is the ID frequency generated by the upper 4-bit RFID tag antenna, distributed between 3 GHz and 5 GHz, and consists of four resonant frequencies. The second set of resonant frequencies is produced by the CMPA. Due to the double resonance characteristic of the shaped circular patch antenna, the dual-resonant frequency is generated, and the front and rear resonant frequency points correspond to the detection of the lateral stress and the longitudinal stress of the structure. By adjusting the size of the antenna so that the resonant frequency of the two separate and non-interfering.

In the strain simulation of 2.1.3, due to the objective existence of the coupling effect, the resonant frequency of the RFID tag will slightly drift with the offset of the resonant frequency of the lower double resonant circular patch antenna. First, the resonant frequency is globally offset. Second, the offset of the ID frequency is still within the measurable range.

A 4-bit resonant frequency tag population is distributed between 3 GHz to 5 GHz, which is divided into four frequency bands, 500 MHz as the frequency range, as illustrated

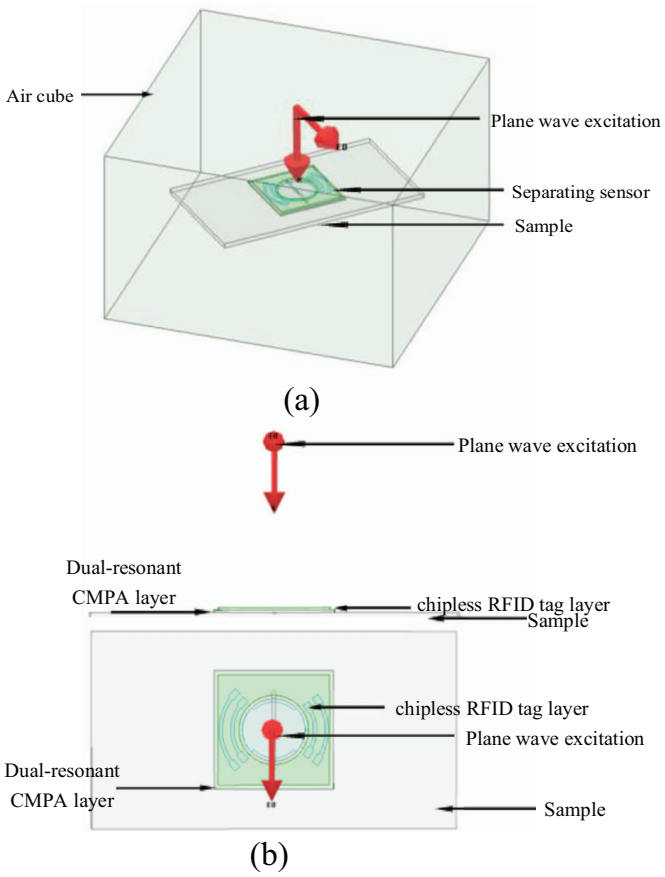

Figure 4. Schematic diagram of the sensor (a) the sensor in air cube; (b) front view and top view of the sensor.

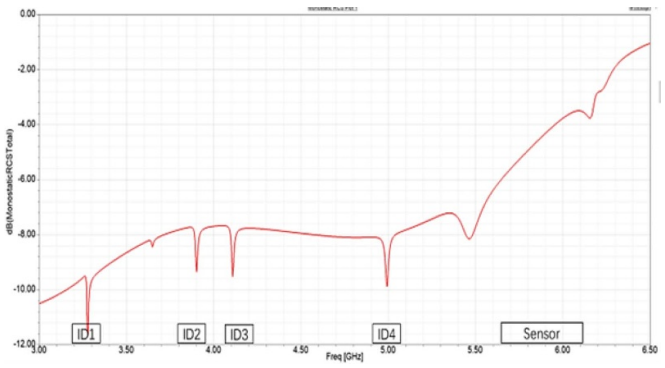

Figure 5. The monostatic radar cross section (RCS) of the two-layer sensor in a wide range.

in figure 5. The ID of the resonant frequency is defined as 1 and the non-resonant frequency is 0. The ID information of the tag is 1111. For 4-bit chipless RFID tags, the maximum amount of information carried is $2^4 = 16$. Increasing the amount of information, a tag can store can be achieved by adding more bits. However, it increases the overall size of the two-layer sensor and occupies a larger bandwidth. If the divided frequency band range is reduced, although the entire working bandwidth can be guaranteed to be constant, bit errors will still occur and the reliability of the sensor will decrease. Considering that both of the RFID note information and the sensor measurement information are included in the entire bandwidth, the number of tag bits is not increased.

2.1.2. Mode analysis and circuital equivalence. Through the current distribution of the circular patch antenna and the RFID tag antenna, we perform modal and equivalent-circuit analysis of the two-layer sensor. According to the circular resonant cavity throry, the circular patch antenna can be equivalent to a resonant cavity, and the current distribution diagrams of its main working mode (cut-off frequency, that is, the first frequency) and secondary working mode (second resonant frequency) are respectively represented as figures 6(a) and (b). Since the surface current distribution of the two resonant frequencies of the circular microstrip antenna is different (The curretn of the second resonant frequency flows in all directions while the current of the first resonant frequency flows in only one direction), it is preliminarily concluded that when the antenna structure is strained, the two resonant frequencies will change differently, which means different frequency drift will occur. The difference between the two resonant frequency changes is described in detail below. The ordinary circular patch antenna is improved, and sectors of different radius are added on the original circular shape for pattern replenishment, which brings dual resonant characteristics to the strain antenna. The dual resonant characteristics is caused by the current distribution generated by the diagonally flowing current of the profiled circular patch. As illustrated in figure 5, the initial front resonant frequency point is in 5.5 Ghz, and the initial rear resonant frequency point is in 6.2 Ghz.

To further understand the dual resonant characteristics, it is possible to observe the surface current distribution of the patch at the front and rear resonance frequencies. Here we separately observe the current distribution of the improved patch antenna.

As illustrated in figure 6(a), the surface current corresponding to the front resonant frequency point is laterally distributed from the middle to both sides. The current intensity is weak in the middle and the color is blue, and the current intensity is strong in both sides, and the colors are yellow and red. Therefore, the front resonant frequency point can characterize the lateral force of the patch antenna.

As illustrated in figure 6(b), the surface current corresponding to the rear resonant frequency point is longitudinally distributed from the middle to both sides, The current intensity is weak in the middle and the color is blue, and the current intensity is strong in both sides, and the colors are yellow and red. Similarly, the rear resonant frequency point can characterize the longitudinal force of the patch antenna.

The 4-bit RFID tag antenna of the tag-layer adopts the design of the improved dipole antenna. In this paper, the 4-bit tag carries information with 1111 as an example. The resonant frequency points of the four tags range from low to high at 3.2804 GHz, 3.902 GHz, 4.1083 GHz, and 4.9931 GHz, respectively. The current distribution of the RFID tag is shown in the figure 7, and it can be seen that as the angle (i.e. length) decreases, the resonant frequency increases.

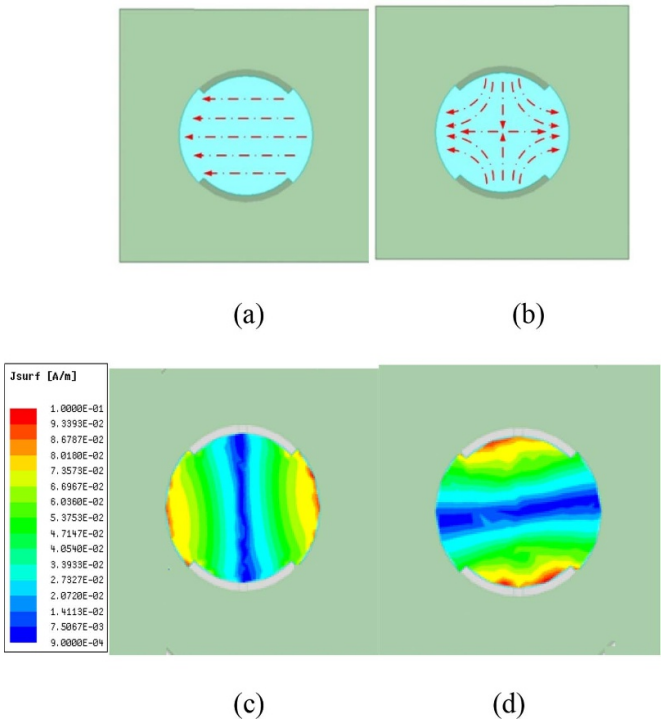

Figure 6. (a) current distribution diagram of its main working mode (b) second working mode (c) current distribution at the initial front resonant frequency point; (d) current field distribution at the initial front resonant frequency point.

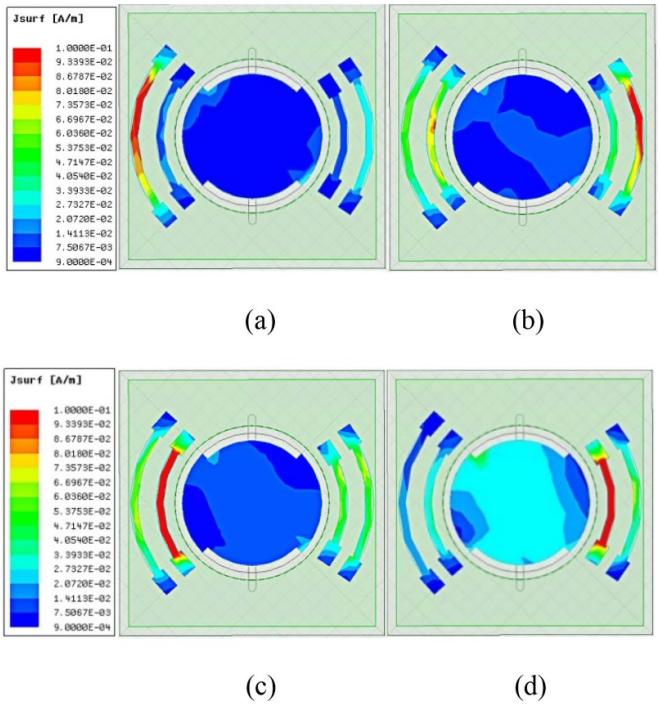

Figure 7. Current distribution of RFID tag (a) current distribution at ID1 resonant frequency point; (b) current distribution at ID2 resonant frequency point; (c) current distribution at ID3 resonant frequency point; (d) current distribution at ID4 resonant frequency point.

For the proposed separating sensor with two layers, the layer of the RFID tag and the layer of strain sensor. The equivalent circuit proposed in this paper is shown in figure 3, and the impedance can be divided into three parts: the impedance of tag-layer Z_{tag} the impedance of CMPA-layer Z_{CMPA} coupling capacitance between the upper and lower patches. The input impedance of separating sensor with two layers can be calculated as:

$$Z_{\text{in}} = Z_{\text{tag}} + Z_{\text{CMPA}} + \frac{1}{\text{j}\omega_o C_o} \tag{4}$$

where the third term in the right side of equation (4) represents the capacitive reactance of the capacitor X_{C_o} which can be described as $\frac{1}{\text{j}\omega_o C_o}$

The 4-bit RFID tag works at the resonant frequency ω_i, where $i = 1, \cdots, n$. Since the RFID tag designed in the paper works in four frequency bands, n is equal to 4. The input impedance of tag-layer consists of a network of n parallel RLC resonators, which can be calculated as:

$$Z_{\text{tag}} = \sum_{i=1}^{n} Z_i = \sum_{i=1}^{n} \frac{1}{G_i + \text{j}(\omega_i C_i - \frac{1}{\omega_i L_i})} \tag{5}$$

The CMPA strain sensor has dual resonant characteristics that can simultaneously excite TM_v and TM_{v_1} The detailed equivalent circuit of the lower layer is illustrated in figure 8(b). Based on the above analysis, the equivalent circuit is simulated in ADS, which is illustrated in figure 8(c). The effect of High Order Mode can be represented by a synthetic small inductance L. The equivalent circuit of lower strain sensor includes two RLC parallel resonant circuits and one series inductor. Since the parameters in each mode depend on the resonant frequency, the impedance of the dual resonant frequency of the strain sensor is equivalent to the sum of Z_v and Z_{v_1}

The input impedance Z_{CMPA} of the circuit in Box can be expressed as:

$$\begin{aligned} Z_{\text{CMPA}} &= Z_v(\omega) + Z_{v_1}(\omega) + Z_\infty(\omega) = R_v(\omega) + R_{v_1}(\omega) + j\omega L \\ &= \frac{1}{G_v + j\left(\omega_v C_v - \frac{1}{\omega_{v_1} L_{v_1}}\right)} + \frac{1}{G_{v_1} + j\left(\omega_{v_1} C_{v_1} - \frac{1}{\omega_{v_1} L_{v_1}}\right)} \\ &\quad + j\omega L \end{aligned} \tag{6}$$

2.1.3. Strain simulation and results analysis. In the Ansoft HFSS simulation, Optimetrics was selected for optimization design to simulate the measurement of the lateral and longitudinal strain of the sensor. We set the transverse stretching distance to v and the longitudinal stretching distance to v_1. As shown in the figure 9, the tensile distance of the CMPA-layer strain sensor is used instead of the actual lateral and longitudinal strain.

Due to the characteristics of the dual resonant circular patch antenna as a strain sensor, the dual resonant frequency points correspond to the force characteristics in different directions. As illustrated in figure 10(a), in the lateral stretching, the front resonant frequency point shifts to the left as the amount of stretching increases, that is, decreases, and the rear

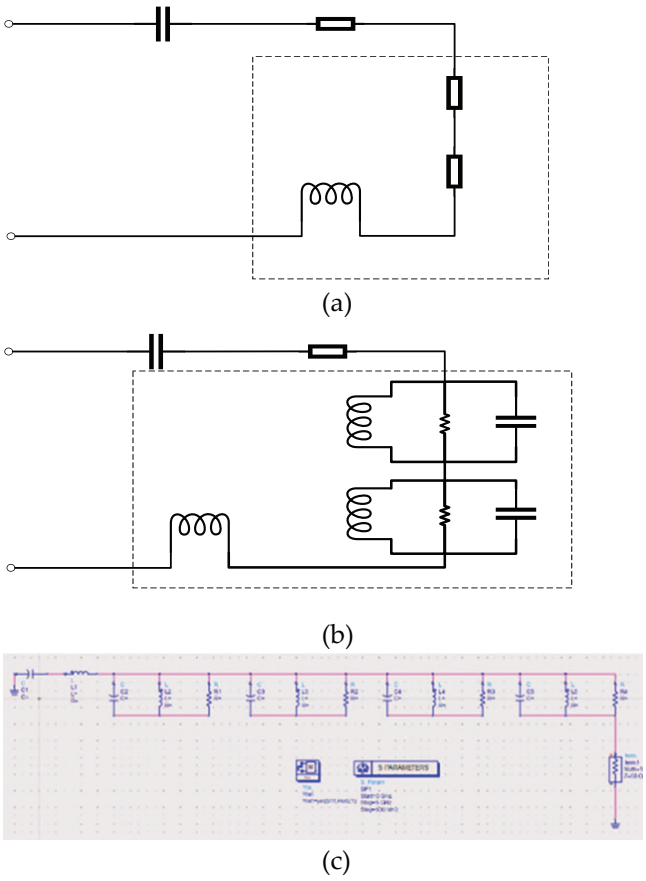

Figure 8. The equivalent circuit of separating sensor with two layers (a) concise schematic (b) detailed schematic with RLC parallel circuit (c) simulation of the equivalent circuit in ads.

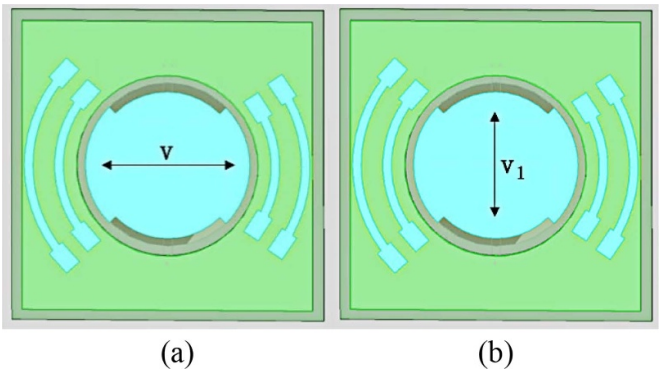

Figure 9. (a) Schematic diagram of the lateral strain simulation; (b) schematic diagram of the longitudinal strain simulation.

resonant frequency point remains basically unchanged. Correspondingly, as illustrated in figure 10(b), in the longitudinal stretching, the rear resonant frequency point shifts to the left as the amount of stretching increases, that is, decreases, while the front resonant frequency point remains substantially unchanged. Due to the deformation of the lower circular patch antenna sensor, the surface current distribution changes, and the resonant frequency of the tag also shifts. However, due to

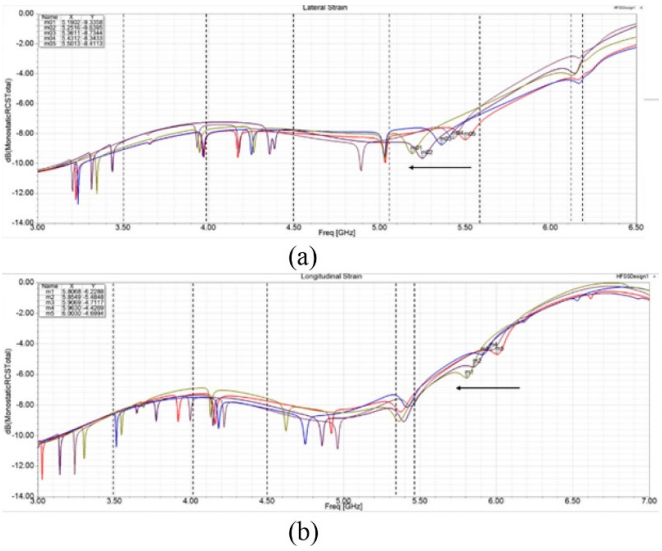

Figure 10. The monostatic radar cross section (RCS) of the sensor with two layers in a wide range (a) variation of resonant frequency during lateral strain simulation; (b) variation of resonant frequency during longitudinal strain simulation.

the wide setting of the RFID tag frequency band, the ID resonant frequency remains within the frequency band of each tag bit.

According to the above characteristics, the magnitude and direction of strain can be detected simultaneously in a passive wireless manner. The resonant frequency point of the sensor part is extracted in the RCS curve, and the relationship between the stress stretching distance and the resonant frequency is plotted, as illustrated in figure 11. The effective measurement range is specified at around 1 mm. According to the fitting result, when lateral strain occurs, the sensitivity coefficient of the strain sensor is 0.4009 Ghz per millimeter, which translates into micro-strain, i.e. 400.9 MHz ε^{-1}. Correspondingly, as illustrated in figure 12, when longitudinal strain occurs, the sensitivity coefficient of the strain sensor is 0.2503 Ghz per millimeter, which translates into micro-strain, i.e. 250.3 MHz ε^{-1}. At the same time, the correlation coefficient of the fitted line is above 0.99, which has a good linear relationship.

As we can see from diagrams above, the dual-resonant CMPA can detect the strain in different directions. Since the CMPA part has two resonant frequencies, when lateral stress is implemented on the sensor, the lower resonant frequency will decrese. When stress causes longitudinal strain, the higher resonant frequency will decrese. Judging from the shift of different frequencies, we can approximately know the direction of the stress.

2.2. *Broadband antenna for transmission and reception*

After designing a sensor system consisting of a separating chipless RFID tag and a strain sensor, it is also necessary to design a corresponding transmitting and receiving antenna for the sensor to work normally [25–27]. Since the split sensor is composed of the RFID tag part and the strain sensor part, the

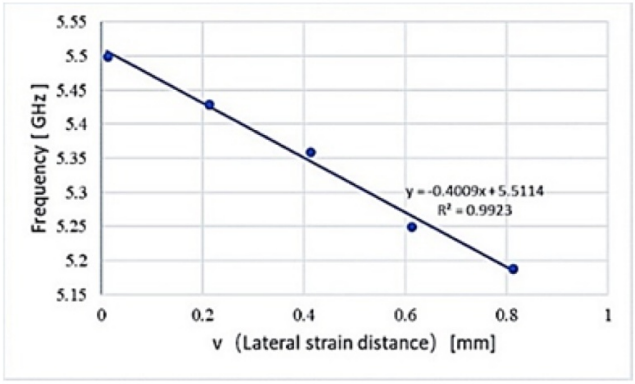

(a)

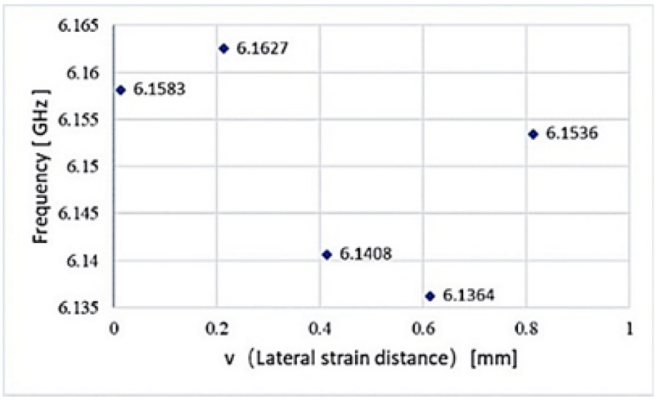

(b)

Figure 11. Relationship between resonant frequency and lateral strain distance (a) the front resonant frequency point of CMPA; (b) the rear resonant frequency point of CMPA.

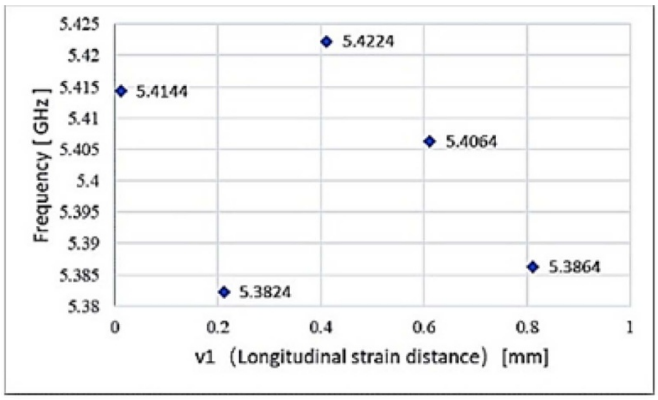

(a)

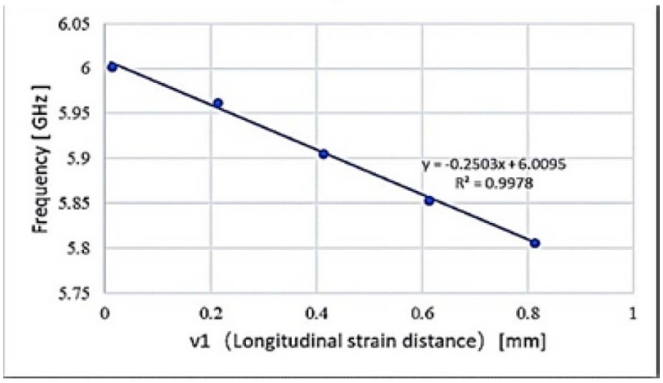

(b)

Figure 12. Relationship between resonant frequency and longitudinal strain distance (a) the front resonant frequency point of CMPA; (b) the rear resonant frequency point of CMPA.

working bandwidth is also superimposed by two parts, so the total working bandwidth requirement is wide. And the broadband antenna needs to be separately designed.

The broadband antenna for transmission and reception proposed in this paper is a disc monopole, including the front disc and the microstrip line, and the ground plate on the back, as illustrated in figure 13.

Observe the performance of the antenna by observing the surface current distribution of the antenna. Obtained from the return loss in the figure 14, the antenna resonates at these two points, 2.95 GHz and 4.3 GHz, respectively, i.e. 2.95 GHz is the first resonant point and 4.3 GHz is the second resonant point.

The antenna current distribution at different frequency points is shown in the figure 15, and the current distribution of the antenna operating at two different frequency points is shown.

As illustrated in figure 15(a), when the antenna operates at the first resonant point, the surface current is mainly distributed at the end of the microstrip line and the edge of the disc, but the current is weak, and the size of the disc affects the first resonance point of the antenna.

As illustrated in figure 15(b), when the antenna operates at the second resonant point, the surface current is mainly distributed in the upper part of the microstrip line, especially from the position where the ground plate intersects to the position where the middle of the microstrip line is the strongest. This shows that the width of the ground plane has a decisive influence on the current distribution and performance of the entire broadband antenna. By changing the size of the disk, the width of the grounding plate and the size of the microstrip line, the parameters of the broadband antenna are adjusted to improve the antenna performance to meet the requirements of wireless measurement.

3. Experiment

3.1. Antenna production by etching

First of all, the antenna was fabricated in our laboratory, and the RFID tag antenna, sensor antenna, and broadband antenna for transmission and reception were physically fabricated using an etching process. As illustrated in figure 16, (a) is an overlay and an exploded view of the entire sensor, (b) is the front and back of the broadband antenna, and the broadband antenna in the figure has been soldered with a coaxial line. The fabricated antenna basically meets the simulation performance requirements.

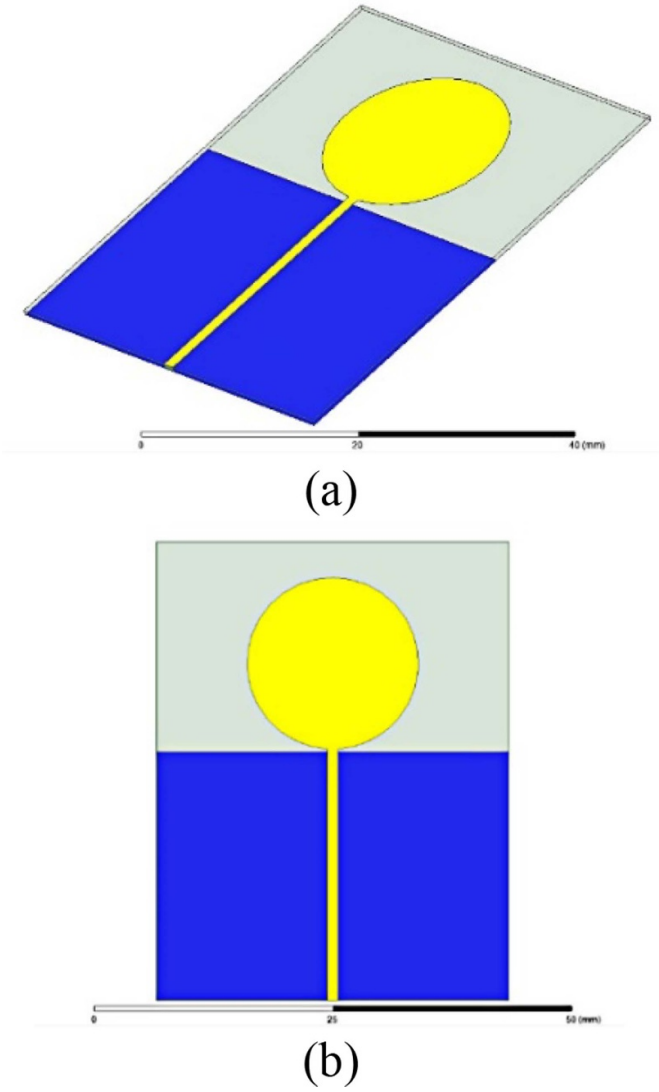

Figure 13. (a) Structure of the disc monopole antenna; (b) exploded view of antenna.

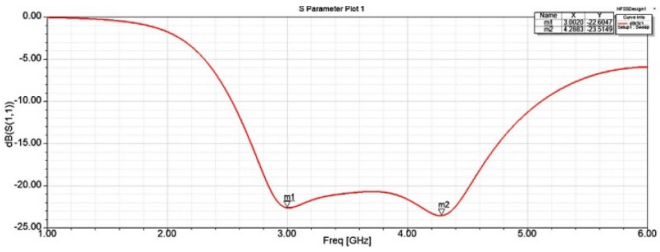

Figure 14. The return loss curve of the broadband antenna in a wide range.

3.2. Instrumentation setup and strain experiment arrangement

The broadband antenna is connected to the VNA by coaxial cable. The VNA model used in the experiment is Keysight N5227A Network Analyzer (Keysight Technologies, Santa Rosa, CA, USA), as illustrated in figure 18. Due to the complexity of the wireless measurement environment and

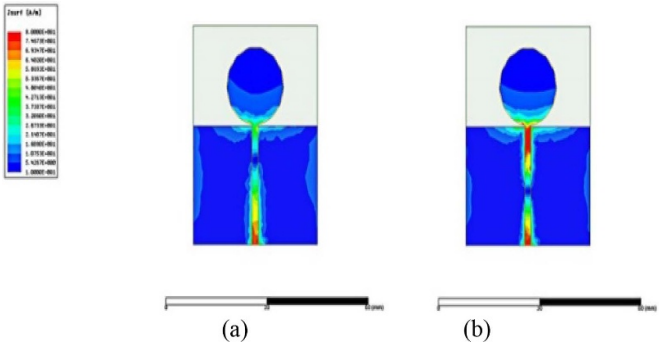

Figure 15. Current density distribution of the broadband antenna: (a) $f = 2.95$ GHz; (b) $f = 4.3$ GHz.

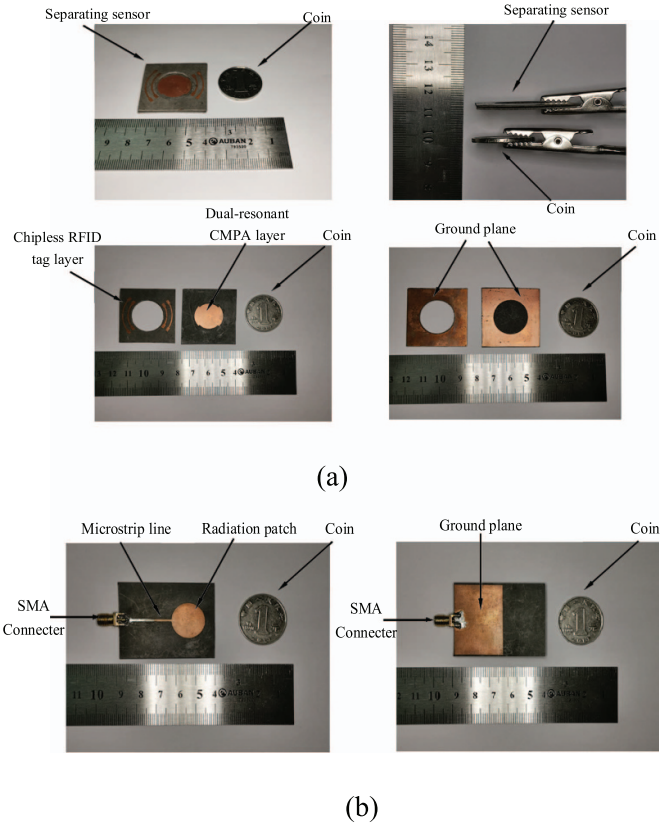

Figure 16. The manufactured antenna: (a) RFID tag antenna and sensor antenna; (b) broadband antenna.

the objective presence of background noise, the broadband antenna is as close as possible to the two-layer sensor to reduce interference. Observing the RCS curve through the VNA optimizes the entire inspection with two layers.

As illustrated in figure 17, the tensile test of the test piece and the measurement of the antenna resonant frequency are performed in an anechoic chamber, and a force gauge is used to measure the tensile force of the aluminum plate. Using the material parameters of the aluminum plate, it is converted into calculation of the strain on the surface of the aluminum plate, which is converted into the lateral and longitudinal strain of the antenna. Starting from 0 kN, the tensile force is applied to the test piece at a span of 3 kN and the actual tensile force value is

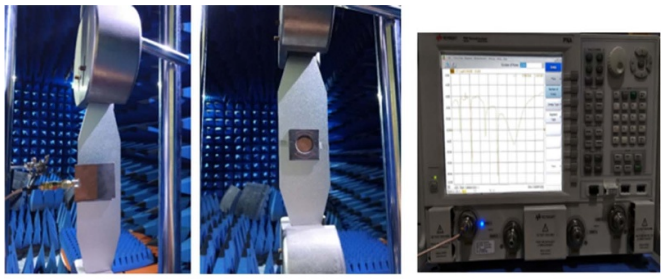

(a) (b) (c)

Figure 17. (a) Broadband antenna setup, facing two-layer sensor; (b) sensor strain experiment setting in anechoic chamber; (c) VNA result display.

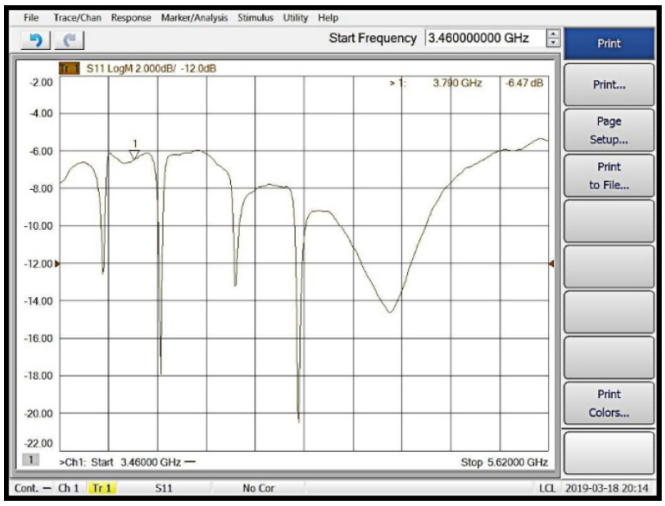

Figure 18. The monostatic radar cross section (RCS) of the sensor with two layers in a wide range from VNA.

recorded after the dynamometer reading is stabilized. Recording starts from 3 kN until the tension increases to 18 kN. Repeat the experiment several times and take the average.

3.3. Results analysis of strain experiment

As illustrated in figure 18, the 4-bit ID bit resonant frequency point and the front and rear resonant frequency points of the dual resonance sensor can be clearly seen in the RCS curve. The resonant frequency of the rear frequency point is shallow and not obvious enough. The reason is mainly that the broadband antenna has a lower performance at higher frequencies, and the post-resonance frequency point of the strain sensor is originally shallower than the former resonance frequency in the simulation.

As illustrated in figure 19, specific experimental data based on conversion of transfer efficiency can be obtained as follows: When lateral strain occurs, the sensitivity coefficient of the strain sensor is 528 $MHz\ \varepsilon^{-1}$, and correlation coefficient is 0.9284. When longitudinal strain occurs, the sensitivity coefficient of the strain sensor is 384 $MHz\ \varepsilon^{-1}$ and correlation coefficient is 0.9235. The sensitivity coefficient unit changed from

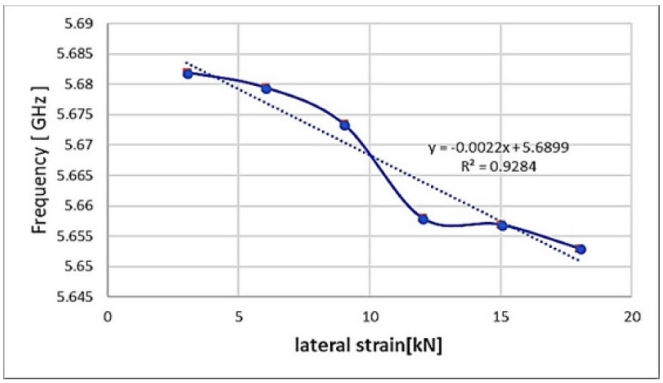

(a)

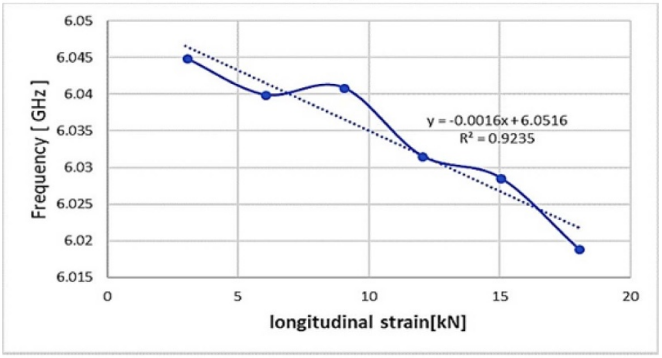

(b)

Figure 19. (a) Relationship between resonant frequency and lateral strain; (b) relationship between resonant frequency and longitudinal strain.

GHz per kN to $MHz\ \varepsilon^{-1}$. The linearity of the experimental data is still good, and it has a certain agreement with the simulation results, but the sensitivity difference of the experiment is quite different from the simulation results. The reasons for the difference may come from the following aspects.

(a) The Monostatic RCS is set to the ideal plane wave excitation in the simulation, but in the actual test, the broadband antenna is connected to the VNA for measurement. The radiation power may have a large gap with the simulation, which has a great impact on the experimental sensitivity. The broadband antenna for transmission and reception and sensor antenna with two layers form a system, so the measured resonant frequency is no longer the resonant frequency of the antenna being measured but the resonant frequency of the entire system. At the same time, the inquiry distance of the Monostatic RCS is set to 10 mm during the simulation. In the actual experiment process, the test distance is 3–5 mm due to the limited conditions of broadband antenna. And the measurement method should be improved later. Errors in detection can be reduced to restore the true information of the sensor antenna by using a new reader.

(b) The patch antenna produced in the laboratory is not sufficient in fineness and may be different from the ideal structure of the simulation. Behind the need to improve the

production process and production accuracy, reduce system errors.

(c) Although the experiment was done in a anechoic chamber, the wireless measurement was greatly disturbed by the environment, and aluminum plates, stretching machines, fixtures, and other metal devices would cause electromagnetic interference to the wireless detection system, affecting the experimental results. The next step is to improve the test algorithm and accuracy, and perform test experiments in the actual environment, in contrast to the measurements in the anechoic chamber.

4. Conclusions

This paper innovatively presents a dual-resonant CMPA sensor with chipless RFID tag for strain detection. The separated layers structure will minimize the influence on the tag layer when strain is implemented. The dual resonant frequency can detect the direction and the amplitude of the strain. Using current distribution analysis and circuital equivalence, the strain size and direction are both studied and a good correlation coefficient was obtained. The sensitivity coefficient of lateral and longitudinal strain is 528 *MHz* ε^{-1} and 384 MHz ε^{-1} on average. The correlation coefficients are 0.9284 and 0.9235 respectively. In the future, we should test the algorithm for improvement and improve the detection device, such as replacing the combination of broadband antenna and VNA with a smart integrated portable reader.

Acknowledgments

This work was supported by the National Natural Science Foundation of China with the Project No. 61671328 and the Fundamental Research Funds for the Central Universities with the Project No. 22120170153.

ORCID iDs

Guochun Wan https://orcid.org/0000-0003-0521-1176
Wenzhao Li https://orcid.org/0000-0002-4346-3035
Mengmeng Li https://orcid.org/0000-0002-0620-8852
Liyu Xie https://orcid.org/0000-0001-5777-0645
Lan Chen https://orcid.org/0000-0002-5747-7761

References

[1] Zhang J, Tian G Y, Marindra A M J, Sunny A and Zhao A 2017 A review of passive RFID tag antenna-based sensors and systems for structural health monitoring applications *Sensors* **17** 265
[2] Huang H 2013 Flexible wireless antenna sensor: a review *IEEE Sens. J.* **13** 3865–72
[3] Mohammad I, Gowda V, Zhai H and Huang H 2011 Detecting crack orientation using patch antenna sensors *Meas. Sci. Technol.* **23** 015102
[4] Xu X and Huang H 2011 Multiplexing passive wireless antenna sensors for multi-site crack detection and monitoring *Smartmater. Struct.* **21** 015004
[5] Caizzone S, DiGiampaolo E and Marrocco G 2014 Wireless crack monitoring by stationary phase measurements from coupled RFID tags *IEEE Trans. Antennas Propag.* **62** 6412–9
[6] Occhiuzzi C, Paggi C and Marrocco G 2011 Passive RFID strain-sensor based on meander-line antennas *IEEE Trans. Antennas Propag.* **59** 4836–40
[7] Kim J, Wang Z and Kim W S 2014 Stretchable RFID for wireless strain sensing with silver nano ink *IEEE Sens. J.* **14** 4395–401
[8] Rakibet O O, Rumens C V, Batchelor J C and Holder S J 2014 Epidermal passive RFID strain sensor for assisted technologies *IEEE Antennas Wirel. Propag. Lett.* **13** 814–7
[9] Mahmoud A M, Ammar H H, Mukdadi O M, Ray I, Imani F S, Chen A and Davalos J F 2010 Non-destructive ultrasonic evaluation of CFRP–concrete specimens subjected to accelerated aging conditions *Ndt & E Int.* **43** 635–41
[10] Chintalapudi K, Fu T, Paek J, Kothari N, Rangwala S, Caffrey J, Govindan R, Johnson E and Masri S 2006 Monitoring civil structures with a wireless sensor network *IEEE Internet Comput.* **10** 26–34
[11] Caizzone S and DiGiampaolo E 2015 Wireless passive RFID crack width sensor for structural health monitoring *IEEE Sens. J.* **15** 6767–74
[12] Watters D G *et al* 2002 Design and performance of wireless sensors for structural health monitoring *AIP Conf Proc.* pp 969–76
[13] Daliri A, Galehdar A, John S, Wang C H, Rowe W S T and Ghorbani K 2012 Wireless strain measurement using circular microstrip patch antennas *Sensors Actuators* A **184** 86–92
[14] Mohammad I and Huang H 2010 Monitoring fatigue crack growth and opening using antenna sensors *Smart Mater. Struct.* **19** 055023
[15] Mohammad I and Huang H 2011 An antenna sensor for crack detection and monitoring *Adv. Struct. Eng.* **14** 47–53
[16] Cho C, Yi X, Li D, Wang Y and Tentzeris M M 2016 Passive wireless frequency doubling antenna sensor for strain and crack sensing *IEEE Sens. J.* **16** 5725–33
[17] Merilampi S, Björninen T, Ukkonen L, Ruuskanen P and Sydänheimo L 2011 Embedded wireless strain sensors based on printed RFID tag *Sens. Rev.* **31** 32–40
[18] Marindra A M J and Tian G Y 2019 Multiresonance chipless RFID sensor tag for metal defect characterization using principal component analysis *IEEE Sens. J.* **19** 8037–46
[19] Ahbe D, Beer S, Zwick T, Wang Y and Tentzeris M M 2012 Dual-band antennas for frequency-doubler-based wireless strain sensing *IEEE Antennas Wirel. Propag. Lett.* **11** 216–9
[20] Thai T T *et al* 2011 Design of a highly sensitive wireless passive RF strain transducer *2011 IEEE MTT-S Int. Microwave Symp.* (IEEE) pp 1–4
[21] Thai T T, Aubert H, Pons P, DeJean G, Tentzeris M M and Plana R 2013 Novel design of a highly sensitive RF strain transducer for passive and remote sensing in two dimensions *IEEE Trans. Microw. Theory Tech.* **61** 1385–96
[22] Marindra A M J, Sutthaweekul R and Tian G Y 2018 Depolarizing chipless RFID sensor tag for characterization of metal cracks based on dual resonance features *2018 10th Int. Conf. on Information Technology and Electrical Engineering (ICITEE)* (IEEE) pp 73–78
[23] Marindra A M J and Tian G Y 2018 Chipless RFID sensor tag for metal crack detection and characterization *IEEE Trans. Microw. Theory Tech.* **66** 2452–62
[24] Balanis C A 2016 *Antenna Theory: Analysis and Design* (New York: Wiley)

[25] Sun X B *et al* 2012 A planar circular disc monopole antenna with improved bandwidth *Microw. Opt. Technol. Lett.* **54** 593–5
[26] Preradovic S and Karmakar N C 2009 Design of short range chipless RFID reader prototype *2009 Int. Conf. on Intelligent Sensors, Sensor Networks and Information Processing (ISSNIP)* (IEEE) pp 307–12
[27] Abbosh A M and Bialkowski M E 2008 Design of ultrawideband planar monopole antennas of circular and elliptical shape *IEEE Trans. Antennas Propag.* **56** 17–23